Interfacial Ice Density Fluctuations Inform Surface Ice-philicity

Zachariah Vicars,[†,‡] Jeongmoon Choi,[†,‡] Sean M. Marks,[†] Richard C. Remsing,[†] and Amish J. Patel[*,†]

[†]*Department of Chemical and Biomolecular Engineering, University of Pennsylvania*

[‡]*Z.V. and J.C. contributed equally to this paper*

E-mail: amish.patel@seas.upenn.edu

Abstract

The propensity of a surface to nucleate ice or bind to ice is governed by its ice-philicity — its relative preference for ice over liquid water. However, the relationship between the features of a surface and its ice-philicity is not well understood, and for surfaces with chemical or topographical heterogeneity, such as proteins, their ice-philicity is not even well-defined. In the analogous problem of surface hydrophobicity, it has been shown that hydrophobic surfaces display enhanced low water-density (vapor-like) fluctuations in their vicinity. To interrogate whether enhanced ice-like fluctuations are similarly observed near ice-philic surfaces, here we use molecular simulations and enhanced sampling techniques. Using a family of model surfaces for which the wetting coefficient, k, has previously been characterized, we show that the free energy of observing rare interfacial ice-density fluctuations decreases monotonically with increasing k. By utilizing this connection, we investigate a set of fcc systems and find that the (110) surface is more ice-philic than the (111) or (100) surfaces. By additionally analyzing the structure of interfacial ice, we find that all surfaces prefer to bind to the basal

plane of ice, and the topographical complementarity of the (110) surface to the basal plane explains its higher ice-philicity. Using enhanced interfacial ice-like fluctuations as a measure of surface ice-philicity, we then characterize the ice-philicity of chemically heterogeneous and topologically complex systems. In particular, we study the spruce budworm anti-freeze protein (sbwAFP), which binds to ice using a known ice-binding site (IBS) and resists engulfment using non-binding sites of the protein (NBSs). We find that the IBS displays enhanced interfacial ice-density fluctuations and is therefore more ice-philic than the two NBSs studied. We also find the two NBSs are similarly ice-phobic. By establishing a connection between interfacial ice-like fluctuations and surface ice-philicity, our findings thus provide a way to characterize the ice-philicity of heterogeneous surfaces.

1 Introduction

Ice formation is a critical process in many fields like cloud formation,[1–3] cryobiology,[4,5] and the engineering of ice-repellent coatings,[6–10] and is typically facilitated by solid surfaces. The propensity of a surface to nucleate and bind to ice is determined by its ice-philicity,[11] which is its relative preference for ice over liquid water. For a macroscopic surface, ice-philicity can be quantified using the wetting coefficient, $k = \frac{\gamma_{SL}-\gamma_{SI}}{\gamma_{IL}}$, where γ_{IL} is the ice-liquid interfacial tension, and γ_{SL} and γ_{SI} are the solid-liquid and solid-ice interfacial tensions, respectively. The wetting coefficient determines the extent to which ice nucleation barriers are reduced, providing a correspondence between k and the supercooling needed to nucleate ice (freezing efficiency).[11] In part because of this relationship, the freezing efficiency has long been used in experiments to quantify the ability of a surface to nucleate ice.[12–17] Numerous simulation studies have elucidated how features, such as lattice match to ice, polarity, charge distribution, and many others influence the surface ice-philicity.[18–22]

Characterizing the ice-philicity of complex surfaces, which exhibit chemical or topographical heterogeneity, remains challenging. For example, ice nucleation on clay minerals, which

influences cloud formation, is known to occur along highly curved regions of the surface.[23–28] Similarly, bacterial ice-nucleating proteins possess surface curvature and chemical heterogeneity which strongly govern their performance.[29] In the related problem of ice-binding, a particularly salient example is the behavior of anti-freeze proteins (AFP). For an AFP to function, it must first preferentially bind to a growing ice nucleus using an ice-binding site (IBS) and resist engulfment with the non-binding regions of the protein (NBSs). It is expected that for the AFP to function properly, the IBS must be ice-philic and the NBSs must be ice-phobic. Further, the binding free energy of the AFP would depend on the ice-philicity of the IBS, whereas its ability to resist engulfment would depend on the ice-phobicity of the NBSs.[30] Because AFPs are inherently heterogeneous, it is challenging to characterize their ice-philicity.

Several studies support the notion that the structure and interactions of interfacial water are related to surface ice-philicity.[11,31,32] Indeed, Davies et. al. were able to construct a predictive machine learning model for surface freezing efficiency using the room-temperature structure of hydration water alone.[33,34] Studies of anti-freeze proteins have likewise focused on understanding the local ordering of hydration water both on and away from the IBS.[35–44] Some studies of bacterial ice-nucleating proteins similarly focus on the ordering of interfacial water.[45–47] The notion that surface ice-philicity is reflected in the structure and properties of interfacial water molecules near a surface is evocative of results in the related problem of surface hydrophobicity.[48] The key observation is that enhanced low-density fluctuations of water can be used as a molecular measure of surface hydrophobicity, such that the easier it is to form cavities in the immediate vicinity of a surface, the more hydrophobic that surface is. This observation has facilitated the use of interfacial water-density fluctuations for characterizing the hydrophobicity of heterogeneous surfaces, like proteins.[49–55] Building on this foundation, we hypothesize that the surface ice-philicity can be quantified within a similar framework by focusing on ice-like density fluctuations near solid interfaces. In other words, water molecules near an ice-philic surface should more readily sample configurational states

consistent with that of ice.

In this study, we aim to investigate whether ice-like density fluctuations near a solid surface can be a predictor of surface ice-philicity. Using enhanced sampling to drive ice formation in the vicinity of a surface, we first show that the free energy of observing interfacial ice is indeed correlated with the wetting coefficient, k, for a family of benchmark pseudo-ice surfaces. We then explore an fcc system, where we quantify the free energetics of forming ice on the (100), (110), and (111) surfaces. We find that the (110) surface displays the most enhanced interfacial ice fluctuations and is therefore the most ice-philic. In addition to rank-ordering the ice-philicity of the three surfaces, our calculations shed light on the structure of interfacial waters that mediate the interactions between a surface and ice and inform the crystal plane of ice that most favorably with the surface. Interestingly, we find that all surfaces preferentially interact with the basal plane of ice. We attribute the enhanced ice-philicity of the (110) surface to the presence of nano-scale surface corrugations that complement the basal plane of ice. Interfacial ice density fluctuations can also be used to characterize the ice-philicity of surfaces with nanoscale chemical and topographical heterogeneity such as anti-freeze proteins, for which the macroscopic wetting coefficient is not well-defined. Here, we characterize the interfacial ice-density fluctuations in three distinct regions of the spruce budworm AFP(sbwAFP) hydration shell: one containing the IBS and the others containing one NBS each. We find that the protein IBS has enhanced ice-density fluctuations relative to non-binding regions of the protein surface. Interestingly, the two NBSs exhibit similar ice-philicity.

2 Methods

2.1 Order Parameters

Discriminating between ice-like and liquid-like water molecules is difficult, especially near interfaces where water molecules exhibit neighbor deficiency. To accurately count the "true"

ice-like molecules, λ, we implement a two-step methodology that addresses both bulk water and interfacial regions. Initially, we introduce an order parameter, $\tilde{M}_v$, which is a measure of the approximate number of ice-like water molecules in the volume, v. This parameter effectively distinguishes ice-like and liquid-like water molecules in bulk[56] and is based on the $\bar{q}_6$ parameter developed by Lechner and Dellago,[57] with the added constraint that water molecules must possess at least four nearest neighbors and reside within v. Coarse-grained INDUS switching functions are used to define these volumes and constraints.[58] This order parameter is identical to the one used in Marks et al.,[56] and is described in detail in the SI.

We estimate λ by identifying water molecules sandwiched between ice-like molecules and solid surface (ones which are neighbor deficient) as ice-like. While imperfect, computing this quantity for each observed configuration enables us to develop an estimate of the "true" number of ice-like water molecules in the simulation box and more accurately account for any chemical potential contributions to the free energies. Additional water molecules that are counted as ice-like using this procedure are identified as "bridging" water molecules, as they mediate the interactions between a solid surface and an ice crystal. This procedure of computing the number of "true" ice-like water molecules is based on a recent publication by Thosar et. al.[30] and is described in detail in the SI.

2.2 Simulation Details

Molecular simulations are performed using versions of GROMACS modified to bias the crystalline order parameters used in this work. For the pseudo-ice and fcc systems, a modified version of GROMACS 2021.4 is used, and for the sbwAFP simulations, a modified version of GROMACS 2016.3 is used. Simulations are performed using the leapfrog integrator with a time-step of 2 fs. All simulations use the TIP4P/Ice model of water, which is known to accurately capture the density, melting point, enthalpy of fusion, and surface tension of water.[59] All mobile water molecules are constrained using the SETTLE algorithm.[60] A cutoff distance of 1 nm is used for Lennard-Jones and short-ranged electrostatic interactions;

no tail corrections are used. Long-ranged electrostatic interactions are treated using the particle-mesh Ewald (PME) method.[61] All production simulations are carried out in the NPT ensemble at $T = 298$ K and $P = 1$ bar. The stochastic velocity rescale thermostat[62] with a time constant of 0.5 ps is used for all simulations.

For the pseudo ice and fcc systems, the stochastic cell-rescale barostat[63] using a time constant of 10 ps is used. Because the surfaces span the x, y directions, semi-isotropic pressure coupling is used with the compressibility set to zero in the x, y directions and a compressibility of 4.8×10^{-5} bar^{-1} set in the z-direction. Prior to running biased simulations, the systems are energy minimized using a steepest descent algorithm and equilibrated for 500 ps in the NPT ensemble. For AFP simulations, we use the Parrinello-Rahman barostat[64] with a time constant of 4 ps. Since the protein is surrounded by water, isotropic pressure coupling is used with a compressibility of 4.5×10^{-5} bar^{-1}. Prior to running biased simulations, the system is energy minimized using a steepest descent algorithm. The system is then equilibrated for 100 ps in the NVT and 1 ns in the NPT ensemble.

Free energy profiles are constructed using the binless WHAM algorithm[65–67] on sets of umbrella sampled data and are expressed in terms of the approximate number of ice-like water molecules λ. Details of how biased simulations in terms of $\tilde{M}_v$ are used to construct free energies in terms of λ are outlined in the SI. All free energies have the chemical potential contribution subtracted to approximate the free energy profile at $T = 273$ K. We use the notation $\beta F_v(\lambda : \Delta\mu = 0) = \beta F_v(\lambda) - \Delta\mu\lambda$ to express these free energies. As previously reported in Marks et. al.,[56] $\Delta\mu = 0.54 \pm 0.1$ kJ/mol for $T = 298$ K.

2.3 System preparation

Pseudo-ice surfaces are constructed by taking bulk ice and position restraining the water oxygens in a manner consistent with Marks et al.[56] To create surfaces with different polarity, a scaling parameter, α, is used which linearly scales the partial charges on each pseudo-ice atom. When $\alpha = 1$, pseudo-ice has the standard charges of TIP4P/Ice, and when $\alpha = 0$, it

is uncharged. Pseudo-ice surfaces are generated using the GenIce package.[68] The fcc systems are constructed using in-house code which templates a default fcc crystal cell such that the desired plane is orthogonal to the z-axis of the simulation cell. These surfaces are position restrained with a spring constant of 40000 kJ mol^{-1}nm^{-2}. A cubic crystal cell with a unit cell length of $a = 3.9236$ Å, modeled after Platinum,[69] is chosen due to its close lattice match with the basal plane of hexagonal ice. In particular, the nearest-neighbor distance of the Pt atoms ($\frac{a}{\sqrt{2}} = 2.774$ Å) is comparable to the projected distance between water-oxygens along the c-axis (≈ 2.83 Å, manually computed from GenIce structures). The surface is moderately hydrophilic, with $\epsilon_{\text{FCC-OW}} = 1.328$ kJ mol^{-1} and $\sigma_{\text{FCC-OW}} = 0.28507$ nm. In order to observe high-λ states, a bias on the order parameter $\tilde{M}_v$ is applied in a cylindrical observation volume. This observation volume is situated at the midpoint of the top-most layer of pseudo-ice atoms and is exactly 0.8 nm tall (approximately two hydration layers of water) and 3 nm in diameter, encompassing roughly 150 water molecules when $\lambda_v = 0$.

We obtain a crystalized protein structure from the protein data bank (1M8N).[70] The sbwAFP is solvated with 35913 water molecules and 3 chlorine molecules to make the system charge neutral. Protein heavy atoms are position restrained using a spring constant of 1000 kJ mol^{-1}nm^{-2} and the protein is modeled using the AMBER99SB forcefield.[71] To conform to the shape of the protein, the observation volumes for the AFP are constructed via a union of spheres (with radius $r = 0.8$ nm) centered on a set of atoms that we classify as belonging to the IBS, NBS1, and NBS2, as described in the SI.[49,50,72] All observation volumes have roughly 220 water molecules in the hydration shell. More details on the setup for the sbwAFP simulations are available in the SI.

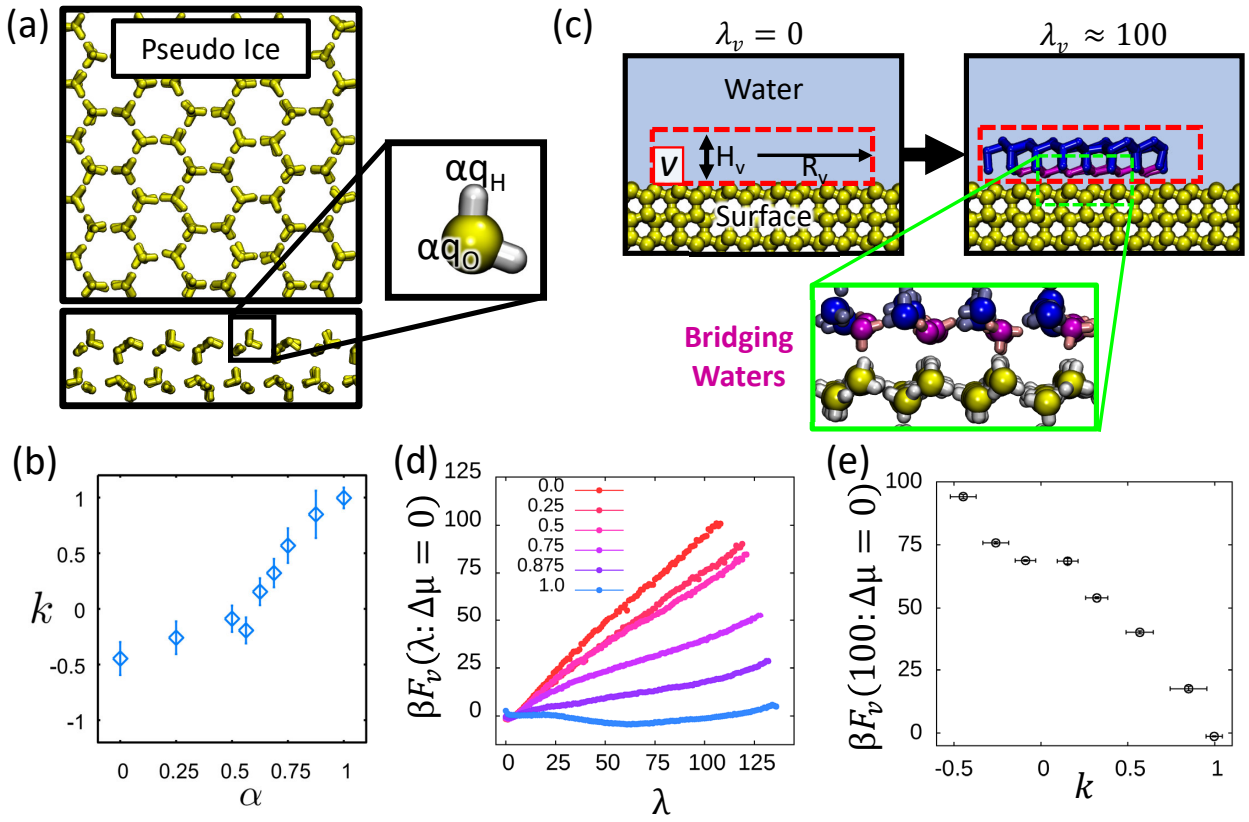

Figure 1: Characterizing the free energetics of ice density fluctuations near the pseudo-ice family of surfaces, which span a wide range of ice-philicities. (a) Pseudo-ice surfaces (yellow) are comprised of TIP4P/Ice water molecules position-restrained to the structure of bulk hexagonal ice. The "polarity" parameter, α, modifies the partial charges on all the surface atoms by a constant factor. (b) The wetting coefficient, k, which quantifies the surface ice-philicity, increases monotonically with α. (reproduced from Marks et. al.)(c) The order parameter, λ_v, counts the number of ice-like water molecules (blue and magenta) in a cylindrical observation volume, v, with radius, $r = 1.5$ nm, and height, $H = 0.8$ nm. In states with low λ (left), no ice is observed, and in states with high λ (right) a thin region of ice appears near the surface. Liquid-like water molecules are omitted for clarity. "Bridging" water molecules, which mediate the interactions between the surface and bulk ice, are shown in the green inset, which shows a typical all-atom representation of the $\alpha = 0.75$ surface. Oxygens of the bridging water molecules are magenta and hydrogens are pink.(d) The free energetics, $F_v(\lambda)$, of observing λ ice-like water molecules in v display fat tails at high λ values. As α increases, high-λ states become more favorable. (e) The free energy required to observe 100 ice-like water molecules in v varies monotonically with the wetting coefficient, suggesting that the free energetics of interfacial ice density fluctuations can serve as a measure of surface ice-philicity.

3 Results and discussion

3.1 Pseudo-ice Surfaces

To test our hypothesis that ice-density fluctuations can serve as a measure of ice-philicity, we employ a family of benchmark surfaces for which the macroscopic wetting coefficient, k, is known. In particular, we use the "pseudo-ice" family of surfaces, which has previously been characterized to understand the impact of surface polarity on k.[56] A family of surfaces with different ice-philicities is constructed by varying the polarity of the pseudo-ice surfaces using a scaling factor α, as shown in Fig. 1(a). Implementation details for these systems are outlined in the methods section. In Fig. 1(b) we show the wetting coefficient, k, as a function of the polarity parameter, α, reproduced from Marks et al.[56] It was found that as α increases so does k, with two different slopes. Between $0 \leq \alpha \leq 0.5$ there is a weak dependence of k on α, followed by a strong dependence in the range $0.5 \leq \alpha \leq 1$. Using this family of systems, we compute the free energy of observing high λ states, which manifest as a thin layer of ice on the surface, as shown in Fig. 1(c). We identify two classes of interfacial ice, with blue water molecules contributing directly to the order parameter $\tilde{M}_v$, and the magenta water molecules, referred to as "bridging waters", which mediate the interactions between the blue, ice-like waters and the surface. We provide a rationale for this approach in the methods section and implementation details in the SI. In the special case of pseudo-ice, the bridging waters essentially look like that of bulk ice, as shown in the green inset panel in 1(c) for $\alpha = 0.75$. However, the structure of the bridging waters is typically unknown a priori, thus an important feature of our method is the ability to implicitly obtain this information from the same biased simulations used to quantify interfacial ice-density fluctuations.

Fig. 1(d) shows the free energy of observing λ ice-like water molecules; we find that as the surface becomes more polar, rare interfacial ice density fluctuations become more favorable. Using the $\alpha = 0.75$ curve as a reference, at low-λ the free energy profile contains a high curvature region, representing the stable, liquid-like configurations of interfacial water

molecules at 298 K. As λ increases, and thus the interfacial water molecules become more ice-like, "fat-tails" can be observed in the free energies. We choose the free energy at $\lambda = 100$ ice-like water molecules to quantify the ease with which rare ice-density fluctuations can be observed. Comparing $F_v(\lambda = 100)$ to k in Fig. 1(e), we find a clear, monotonic relationship between rare ice-density fluctuations and k, suggesting that such fluctuations could serve as a predictor of surface ice-philicity. Encouragingly, relationship between rare ice-density fluctuations and k is analogous to the relationship between interfacial water density fluctuation and surface hydrophilicity, a topic which has been studied in far greater detail in the literature. Just as we observe fat tails in the $F_v(\lambda)$ distributions for ice-philic surfaces, hydrophobic surfaces are known to display fat low-density tails in the number of waters near the surface, suggesting that it is easier to form cavities near these surfaces.[48,50] Several studies have leveraged this insight to characterize hydrophobicity on chemically and/or topographically complex surfaces like heterogeneous SAM surfaces[73] or proteins.[49,51,53,54,72]

3.2 FCC Surfaces

Having established the connection between rare interfacial ice-density fluctuations and k, we now leverage this relationship to quantify the ice-philicity of a set of fcc surfaces. In particular, we seek to uncover if certain planes of the fcc crystal might be more ice-philic than others. To this end, we characterize the ice-density fluctuations in the vicinity of the (100), (110), and (111) planes of the fcc crystal.

Fig. 2(a) shows each of the crystal planes we simulate. The lattice spacing of the fcc crystal is chosen to correspond to the structure of Platinum, whose (111) plane is a near lattice match to that of the basal plane of ice, as detailed in the methods section. The forcefield parameters are tuned to make the surface hydrophilic, with precise values also available in the methods section. Fig. 2(b) suggests that the (110) surface has the fattest tail, followed by the (111) and the (100) surfaces, implying that the (110) surface is the most ice-philic. This is more clearly shown in the bar chart in Fig. 2(c), which shows the values of

the free energy profiles at $\lambda = 100$. Fig. 2(d) reveals that the (110) surface is better able to support the basal plane due to the nano-scale corrugations on the top surface, in contrast to the (111) and (100) surfaces whose interfacial water molecules are constrained to be nearly planar. Surface roughness has previously been found to contribute to ice-philicity in a study of AgI surfaces by Liu and coworkers.[18] All surfaces prefer to nucleate the basal plane of ice, with corresponding prismatic planes visible from the side profiles as shown in Fig. 2(d). This observation is consistent with the work of Fitzner et. al.[74] who similarly observed basal plane nucleation for fcc surfaces with a similar lattice match and hydrophilicity. Interestingly, the (100) plane seems to nucleate with the a-axis of ice offset from the a-axis of the fcc crystal. Plots of $\Delta F(\lambda = 100)$ vs k, along with a comparison with the pseudo-ice family of surfaces are available in the SI.

Such knowledge of the preferred binding plane, orientation, and structure of interfacial ice can be used to facilitate seeding calculations like HSEED[75] and RSeeds,[76] which are used to estimate heterogeneous ice nucleation rates but require candidate ice nuclei, or seeds, to initialize the simulation. In particular, HSEED uses a random structure search to generate seeds, while RSeeds treats an initial ice seed as a pseudo-rigid body and allows it to equilibrate with interfacial water to generate candidate seed configurations. This information is also helpful for initializing SWIPES simulations, which aims to directly estimate k and requires a careful choice of plate size and spacing to avoid the build-up of internal stresses.[56]

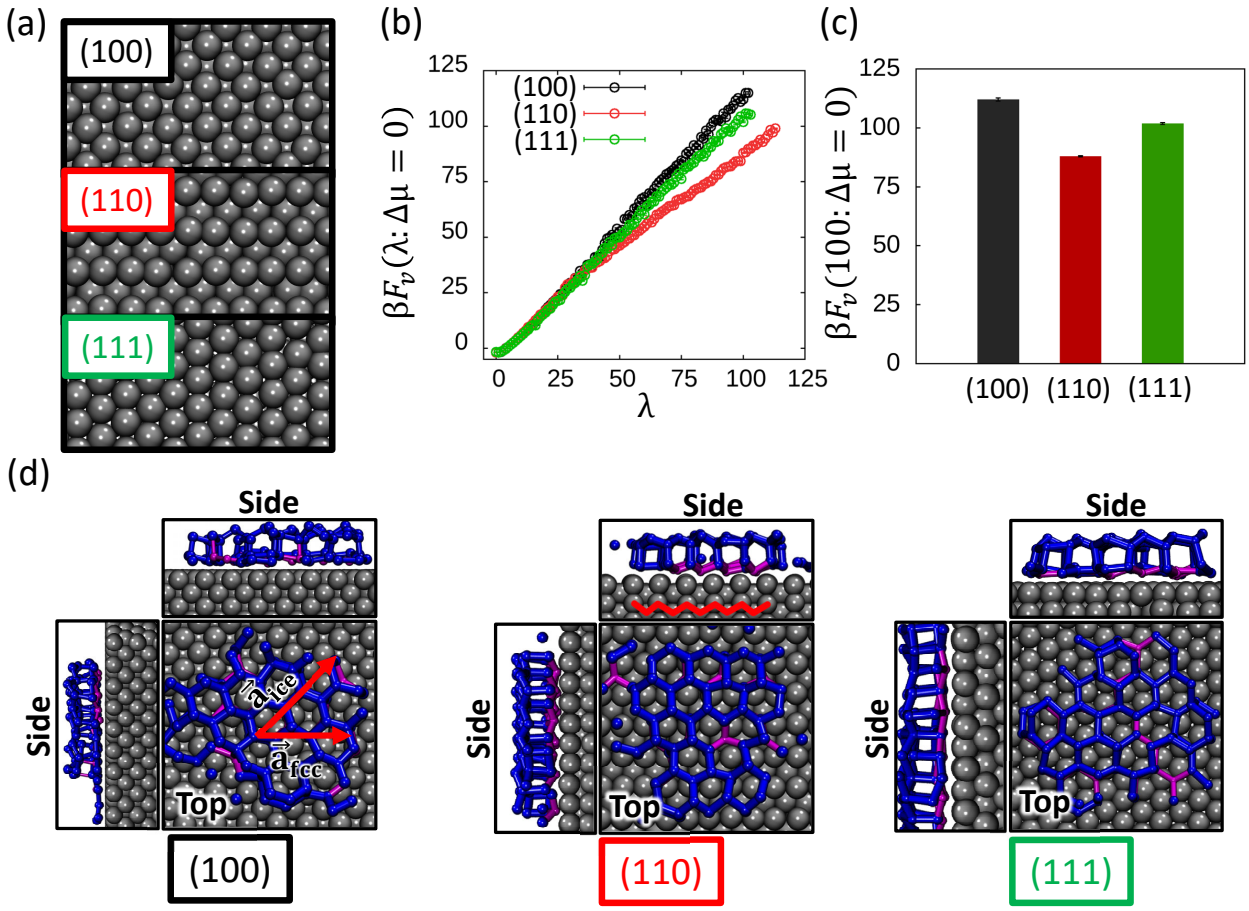

Figure 2: (a) Three planes of an fcc crystal with a lattice constant $a = 3.9236$ Å are studied; surface atoms are shown in gray. (b) The free energetics of ice density fluctuations, $F_v(\lambda)$, near the (110) surface has a fatter tail than the (100) and (111) surfaces, suggesting that the (110) surface is more ice-philic than the other two. (c) The free energy of observing $\lambda = 100$ ice-like water molecules in v suggests that the (110) surface is the most ice-philic followed by the (111) surface, and finally the (100) surface. (d) Selected snapshots for each surface highlight that all surfaces nucleate the basal plane of ice, with the top, and two side views showing the basal, 1st prismatic, and 2nd prismatic planes, respectively. Ice-like water molecules are shown in blue, bridging water molecules are shown in magenta, and liquid-like water molecules are omitted for clarity. Interestingly, the a-axis of ice is aligned with the diagonal (rather than the crystal axis) of the (100) surface (red arrows), whereas the two axes are coincident for the (110) and (111) surfaces. The enhanced ice-philicity of the (110) surface likely stems from corrugations (solid red lines) which better support the basal plane.

3.3 Antifreeze proteins

The relationship between interfacial ice density fluctuations and k can also be used to characterize the ice-philicity of chemically and topographically heterogeneous surfaces, such as proteins. Here we use this relationship to study the spruce budworm AFP (sbwAFP).[77,78] The sbwAFP has three distinct regions; the experimentally revealed ice-binding site (IBS), which binds to the growing ice nucleus, and two non-binding sites (NBSs), which serve to resist engulfment by ice, with each site being associated with a single side of the (approximately) triangular prismatic AFP. In Fig. 3(a), we show the distribution of polar/charged atoms and non-polar atoms on each side of the AFP.[79] Side 1 contains the experimental IBS and possesses stripes of polar residues resulting from TxT motifs, composed of two threonine residues surrounding an arbitrary central residue. This patterning of polar residues is commensurate with the structure of bulk ice.

As the ice-philicity of the IBS is crucial in its ability to selectively bind to ice, we expect it to be ice-philic.[77,80,81] To verify this hypothesis we carry out a set of simulations to calculate the free energy of observing ice-like water molecules in the hydration shell of each side of the protein. The selected atoms for the IBS, NBS1, and NBS2 are illustrated in Fig. 3(b). The corresponding observation volume for the IBS is shown in 3(c). Specific details of the simulation setup are available in the methods, and we describe how we define the IBS and NBSs in the SI. Fig. 3(d) presents the free energy associated with observing λ ice-like molecules within these volumes. We find that high-λ fluctuations are more favorable for the IBS than either NBS1 or NBS2, which suggests that the IBS is more ice-philic than either NBS. This finding is consistent with the expecation that AFPs use their IBS to preferentially bind to a growing ice nucleus.[81] If we focus specifically on the free energy required to have $\lambda = 100$ ice-like water molecules in each observation volume, as shown in Fig. 3(e), we find that there is an $\approx 40\ kT$ difference in $F_v(\lambda = 100)$ between IBS and NBSs. We also find that while NBS2 appears to be slightly more ice-philic than NBS1, the difference between NBS1 and NBS2 is less pronounced than that of either NBS and the IBS. The comparable

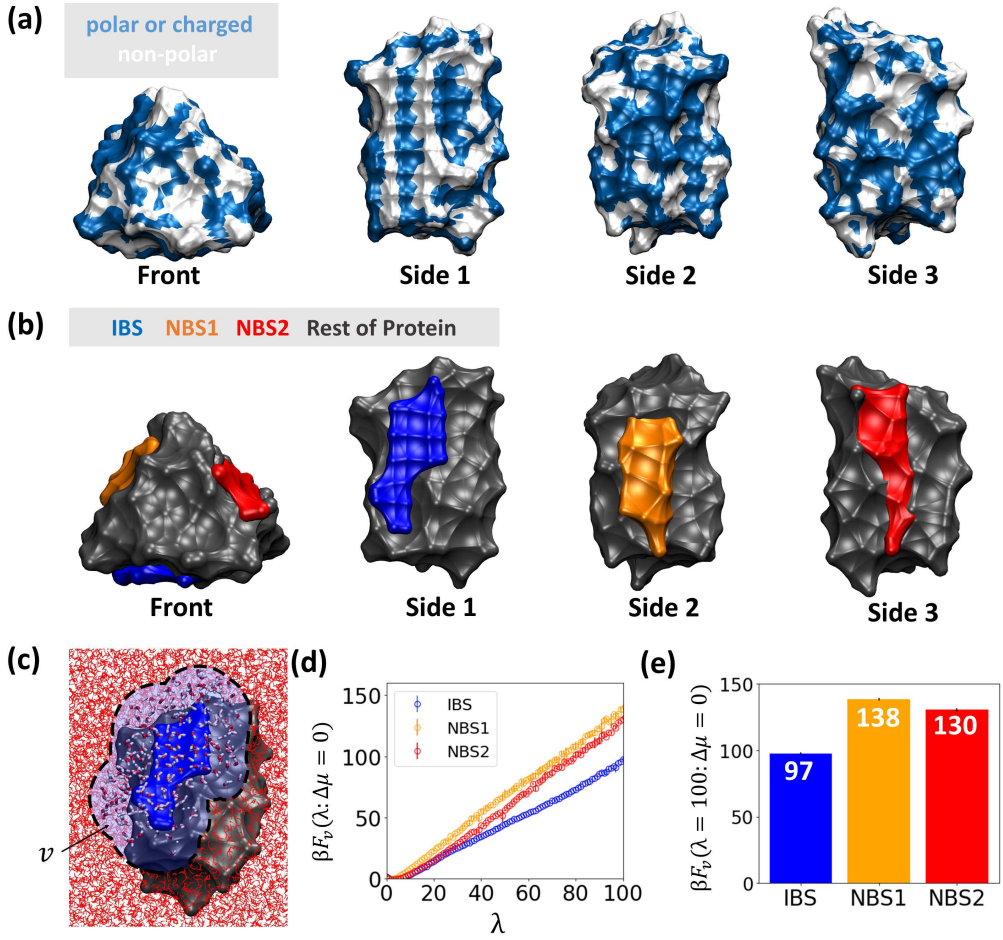

Figure 3: Calculating the free energetics of interfacial ice density fluctuations in the hydration shell of the spruce budworm antifreeze protein (sbwAFP). (a) sbwAFP is chemically and topographically heterogeneous. Polar or charged atoms are colored in blue and non-polar atoms are colored in white. (b) We highlight three regions of interest on the surface of sbwAFP: the ice-binding sites (IBS) and two non-binding sites (NBS1 and NBS2), which are colored blue, orange, and red, respectively. The rest of the protein is colored gray. (c) An observation volume, v (transparent blue region), encompassing water molecules within 0.8 nm of the IBS (licorice) is shown. Water molecules outside the hydration shell are shown in red lines. (d) The free energetics of observing λ ice-like water molecules near the three sides of sbwAFP highlight that high λ states are significantly more favorable near the IBS than NBS1 or NBS2. (e) The free energy of observing $\lambda = 100$ ice-like water molecules in v suggests that the IBS is more ice-philic than either NBS, whereas NBS1 and NBS2 have similar ice-philicities.

free energy profiles of the NBSs suggest a uniform resistance by antifreeze proteins (AFP) to ice formation on both sites. This is in line with results from Marks et. al., which suggests that non-lattice matched surfaces tend to be similarly ice-phobic,[56] with $k = -0.5$. Our results are also consistent with the experiments of Liu et al.,[82] who anchored different AFPs onto solid surfaces with either the IBS or NBS facing the bulk, and found that the NBS was ice-phobic and suppressed ice nucleation to a greater extent than if the IBS is facing the bulk.

4 Conclusions

The ice-philicity, k, of a surface influences its ability to nucleate or bind to ice. However, the relationship between the molecular characteristics of a surface and its ice-philicity is not well understood, especially for heterogeneous surfaces, such as proteins. In this work we elucidate the properties of water molecules near a surface that reflect its ice-philicity. In particular, we use molecular simulations and enhanced sampling techniques to show that ice-density fluctuations are enhanced near ice-philic surfaces, suggesting that such fluctuations could be used as a predictor of surface ice-philicity.

We leverage the connection between ice-density fluctuations and k to characterize the ice-philicity of a set of fcc surfaces and find that the (110) surface is the most ice-philic followed by the (111) and (100) surfaces, respectively. By facilitating the formation of interfacial ice, our simulations additionally provide us with the structure of the waters that mediate the interactions between the surface and ice as well as the plane of ice that interacts most favorably with the surface. We find that all fcc surfaces nucleate the basal plane of ice, and the enhanced ice-philicity of the (110) surface can be attributed to its nanoscale roughness, which is most commensurate with the basal plane. We hope that such information about the ice plane that the surface prefers and the structure of the waters that mediate surface-ice interactions will also serve as a useful starting point for other approaches, such as SWIPES,

which seeks to quantify k, or seeding approaches like HSEED or RSeeds, which are used to predict heterogeneous ice nucleation rates.[56,75,76]

By using interfacial ice-density fluctuations we are able to additionally characterize the ice-philicity of heterogeneous surfaces, like AFPs, which cannot be readily quantified with a unique value of k. In particular, by quantifying the interfacial ice-density fluctuations of sbwAFP near its ice-binding site (IBS) and two non-binding sites (NBSs), we show that the IBS is markedly more ice-philic than either NBS, which is consistent with an AFP's function of binding ice through its IBS and resisting engulfment using its NBS.[81] We emphasize that AFPs are only a subset of the materials for which curvature and chemical heterogeneity play a role in ice nucleation. Atmospheric dust, which is often composed of micro and nanoparticles of feldspar, quartz, kaolinite, and many other naturally occurring materials, is rich in structural heterogeneity and has a substantial effect on cloud formation.[23,26,27] Understanding the thermodynamics of rare interfacial ice-density fluctuations in these systems could shed light on the effectiveness of these materials as atmospheric ice nucleators. In addition, superhydrophobic surfaces, which possess nano-scale surface texture, have been explored as anti-icing surfaces.[6,28] Our approach could be used to identify where and how readily ice nucleates on these materials and could lead to developing more robust ice-repellent coatings by quantifying their ice-philicity.[83]

The structure and thermodynamics of interfacial water/ice are likewise an important consideration in the study of ice friction at the nanoscale.[84–87] In particular, we anticipate that ice-philic surfaces, which display enhanced ice density fluctuations, are less likely to stabilize an interfacial layer of liquid water and consequently have a higher friction coefficient. We believe that the conceptual and methodological framework presented here may also be applicable to other crystal-melt systems, such as clathrate hydrates. Clathrate hydrates tend to form in gas pipelines, where they can cause clogs or damage, as well as within ocean floor sediments, where they play an important role in storing methane.[88–90] Thus, characterizing surface 'clathrate-philicity' by quantifying clathrate-like interfacial fluctuations would be

of immense interest in both industry and climate science. Additionally, clathrate-binding proteins (CBPs) have been recently found as inhibitors of clathrate formation in some ocean-dwelling bacteria,[91] suggesting that our approach might be adapted to gain molecular insights into the function of these proteins.

Acknowledgement

This material is based upon work supported by the U.S. Department of Energy (DOE), Office of Science, Office of Basic Energy Sciences, under Award Number DE-SC0021241. S.M.M. was supported by a DOE Computational Science Graduate Fellowship (DE-FG02-97ER25308). A.J.P. is grateful to the Alfred P. Sloan Research Foundation (FG-2017-9406) and the Camille and Henry Dreyfus Foundation (TC-19-033) for early-career awards.

Supporting Information Available

Supporting Information: Implementation details for $\tilde{M}_v$ and λ_v, a comparison of ΔF vs k for pseudo-ice and fcc surfaces, and additional details for the sbwAFP calculation (PDF)

References

(1) Malik, S.; Bano, H.; Rather, D.-R.; Ahmad, S. Cloud Seeding; Its Prospects and Concerns in the Modern World-A Review. **2018**, *6*.

(2) Slater, B.; Michaelides, A.; Salzmann, C. G.; Lohmann, U. A Blue-Sky Approach to Understanding Cloud Formation. *Bulletin of the American Meteorological Society* **2016**, *97*, 1797–1802.

(3) Chatziparaschos, M.; Daskalakis, N.; Myriokefalitakis, S.; Kalivitis, N.; Nenes, A.; Gonçalves Ageitos, M.; Costa-Surós, M.; Pérez García-Pando, C.; Zanoli, M.; Vrekous-

sis, M.; Kanakidou, M. Role of K-feldspar and quartz in global ice nucleation by mineral dust in mixed-phase clouds. *Atmospheric Chemistry and Physics* **2023**, *23*, 1785–1801.

(4) Liu, X.; Pan, Y.; Liu, F.; He, Y.; Zhu, Q.; Liu, Z.; Zhan, X.; Tan, S. A Review of the Material Characteristics, Antifreeze Mechanisms, and Applications of Cryoprotectants (CPAs). *Journal of Nanomaterials* **2021**, *2021*, e9990709.

(5) William, N.; Acker, J. P. High sub-zero organ preservation: A paradigm of nature-inspired strategies. *Cryobiology* **2021**, *102*, 15–26.

(6) He, Z.; Zhuo, Y.; Zhang, Z.; He, J. Design of Icephobic Surfaces by Lowering Ice Adhesion Strength: A Mini Review. *Coatings* **2021**, *11*, 1343.

(7) Cao, L.; Jones, A. K.; Sikka, V. K.; Wu, J.; Gao, D. Anti-Icing Superhydrophobic Coatings. *Langmuir* **2009**, *25*, 12444–12448.

(8) Latthe, S. S.; Sutar, R. S.; Bhosale, A. K.; Nagappan, S.; Ha, C.-S.; Sadasivuni, K. K.; Liu, S.; Xing, R. Recent developments in air-trapped superhydrophobic and liquid-infused slippery surfaces for anti-icing application. *Progress in Organic Coatings* **2019**, *137*, 105373.

(9) Lin, Y.; Chen, H.; Wang, G.; Liu, A. Recent Progress in Preparation and Anti-Icing Applications of Superhydrophobic Coatings. *Coatings* **2018**, *8*, 208.

(10) Villegas, M.; Zhang, Y.; Abu Jarad, N.; Soleymani, L.; Didar, T. F. Liquid-Infused Surfaces: A Review of Theory, Design, and Applications. *ACS Nano* **2019**, *13*, 8517–8536.

(11) Qiu, Y.; Odendahl, N.; Hudait, A.; Mason, R.; Bertram, A. K.; Paesani, F.; DeMott, P. J.; Molinero, V. Ice Nucleation Efficiency of Hydroxylated Organic Surfaces Is Controlled by Their Structural Fluctuations and Mismatch to Ice. *J. Am. Chem. Soc.* **2017**, *139*, 3052–3064.

(12) Lupi, L.; Hudait, A.; Molinero, V. Heterogeneous Nucleation of Ice on Carbon Surfaces. *J. Am. Chem. Soc.* **2014**, *136*, 3156–3164.

(13) Hiranuma, N.; Adachi, K.; Bell, D. M.; Belosi, F.; Beydoun, H.; Bhaduri, B.; Bingemer, H.; Budke, C.; Clemen, H.-C.; Conen, F.; Cory, K. M.; Curtius, J.; DeMott, P. J.; Eppers, O.; Grawe, S.; Hartmann, S.; Hoffmann, N.; Höhler, K.; Jantsch, E.; Kiselev, A.; Koop, T.; Kulkarni, G.; Mayer, A.; Murakami, M.; Murray, B. J.; Nicosia, A.; Petters, M. D.; Piazza, M.; Polen, M.; Reicher, N.; Rudich, Y.; Saito, A.; Santachiara, G.; Schiebel, T.; Schill, G. P.; Schneider, J.; Segev, L.; Stopelli, E.; Sullivan, R. C.; Suski, K.; Szakáll, M.; Tajiri, T.; Taylor, H.; Tobo, Y.; Ullrich, R.; Weber, D.; Wex, H.; Whale, T. F.; Whiteside, C. L.; Yamashita, K.; Zelenyuk, A.; Möhler, O. A comprehensive characterization of ice nucleation by three different types of cellulose particles immersed in water. *Atmospheric Chemistry and Physics* **2019**, *19*, 4823–4849.

(14) Pinti, V.; Marcolli, C.; Zobrist, B.; Hoyle, C. R.; Peter, T. Ice nucleation efficiency of clay minerals in the immersion mode. *Atmospheric Chemistry and Physics* **2012**, *12*, 5859–5878.

(15) Broadley, S. L.; Murray, B. J.; Herbert, R. J.; Atkinson, J. D.; Dobbie, S.; Malkin, T. L.; Condliffe, E.; Neve, L. Immersion mode heterogeneous ice nucleation by an illite rich powder representative of atmospheric mineral dust. *Atmospheric Chemistry and Physics* **2012**, *12*, 287–307.

(16) Vonnegut, B. The Nucleation of Ice Formation by Silver Iodide. *Journal of Applied Physics* **1947**, *18*, 593–595.

(17) Murray, B. J.; O'Sullivan, D.; Atkinson, J. D.; Webb, M. E. Ice nucleation by particles immersed in supercooled cloud droplets. *Chem. Soc. Rev.* **2012**, *41*, 6519–6554.

(18) Liu, Z.; Li, C.; Goonetilleke, E. C.; Cui, Y.; Huang, X. Role of Surface Templating

on Ice Nucleation Efficiency on a Silver Iodide Surface. *J. Phys. Chem. C* **2021**, *125*, 18857–18865.

(19) Glatz, B.; Sarupria, S. The surface charge distribution affects the ice nucleating efficiency of silver iodide. *J. Chem. Phys.* **2016**, *145*, 211924.

(20) Cox, S. J.; Kathmann, S. M.; Slater, B.; Michaelides, A. Molecular simulations of heterogeneous ice nucleation. I. Controlling ice nucleation through surface hydrophilicity. *The Journal of Chemical Physics* **2015**, *142*, 184704.

(21) Zielke, S. A.; Bertram, A. K.; Patey, G. N. A Molecular Mechanism of Ice Nucleation on Model AgI Surfaces. *J. Phys. Chem. B* **2015**, *119*, 9049–9055.

(22) Zielke, S. A.; Bertram, A. K.; Patey, G. N. Simulations of Ice Nucleation by Kaolinite (001) with Rigid and Flexible Surfaces. *J. Phys. Chem. B* **2016**, *120*, 1726–1734.

(23) Kiselev, A.; Bachmann, F.; Pedevilla, P.; Cox, S. J.; Michaelides, A.; Gerthsen, D.; Leisner, T. Active sites in heterogeneous ice nucleation—the example of K-rich feldspars. *Science* **2017**, *355*, 367–371.

(24) Soni, A.; Patey, G. N. Simulations of water structure and the possibility of ice nucleation on selected crystal planes of K-feldspar. *J. Chem. Phys.* **2019**, *150*, 214501.

(25) Soni, A.; Patey, G. N. How Microscopic Features of Mineral Surfaces Critically Influence Heterogeneous Ice Nucleation. *J. Phys. Chem. C* **2021**, *125*, 10723–10737.

(26) Soni, A.; Patey, G. N. Unraveling the Mechanism of Ice Nucleation by Mica (001) Surfaces. *J. Phys. Chem. C* **2021**, *125*, 26927–26941.

(27) Sosso, G. C.; Li, T.; Donadio, D.; Tribello, G. A.; Michaelides, A. Microscopic Mechanism and Kinetics of Ice Formation at Complex Interfaces: Zooming in on Kaolinite. *J. Phys. Chem. Lett.* **2016**, *7*, 2350–2355.

(28) Roudsari, G.; Reischl, B.; Pakarinen, O. H.; Vehkamäki, H. Atomistic Simulation of Ice Nucleation on Silver Iodide (0001) Surfaces with Defects. *J. Phys. Chem. C* **2020**, *124*, 436–445.

(29) Dolev, M. B.; Braslavsky, I.; Davies, P. L. Ice-Binding Proteins and Their Function. *Annual Review of Biochemistry* **2016**, *85*, 515–542.

(30) Thosar, A. U.; Cai, Y.; Marks, S. M.; Vicars, Z.; Choi, J.; Pallath, A.; Patel, A. J. On the engulfment of antifreeze proteins by ice. *Proceedings of the National Academy of Sciences* **2024**, *121*, e2320205121.

(31) Wu, S.; He, Z.; Zang, J.; Jin, S.; Wang, Z.; Wang, J.; Yao, Y.; Wang, J. Heterogeneous ice nucleation correlates with bulk-like interfacial water. *Science Advances* **2019**, *5*, eaat9825.

(32) Metya, A. K.; Molinero, V. Is ice nucleation by organic crystals nonclassical? An assessment of the monolayer hypothesis of ice nucleation. *Journal of the American Chemical Society* **2021**, *143*, 4607–4624.

(33) Davies, M. B.; Fitzner, M.; Michaelides, A. Accurate prediction of ice nucleation from room temperature water. *Proceedings of the National Academy of Sciences* **2022**, *119*, e2205347119.

(34) Fitzner, M.; Pedevilla, P.; Michaelides, A. Predicting heterogeneous ice nucleation with a data-driven approach. *Nat Commun* **2020**, *11*, 4777.

(35) Hudait, A.; Odendahl, N.; Qiu, Y.; Paesani, F.; Molinero, V. Ice-nucleating and antifreeze proteins recognize ice through a diversity of anchored clathrate and ice-like motifs. *Journal of the American Chemical Society* **2018**, *140*, 4905–4912.

(36) Garnham, C. P.; Campbell, R. L.; Davies, P. L. Anchored clathrate waters bind an-

tifreeze proteins to ice. *Proceedings of the National Academy of Sciences* **2011**, *108*, 7363–7367.

(37) Midya, U. S.; Bandyopadhyay, S. Interfacial Water Arrangement in the Ice-Bound State of an Antifreeze Protein: A Molecular Dynamics Simulation Study. *Langmuir* **2017**, *33*, 5499–5510.

(38) Zielkiewicz, J. Mechanism of antifreeze protein functioning and the "anchored clathrate water" concept. *The Journal of Chemical Physics* **2023**, *159*, 085101.

(39) Grabowska, J.; Kuffel, A.; Zielkiewicz, J. Structure of solvation water around the active and inactive regions of a type III antifreeze protein and its mutants of lowered activity. *The Journal of Chemical Physics* **2016**, *145*, 075101.

(40) Hudait, A.; Moberg, D. R.; Qiu, Y.; Odendahl, N.; Paesani, F.; Molinero, V. Preordering of water is not needed for ice recognition by hyperactive antifreeze proteins. *Proceedings of the National Academy of Sciences* **2018**, *115*, 8266–8271.

(41) Hudait, A.; Qiu, Y.; Odendahl, N.; Molinero, V. Hydrogen-Bonding and Hydrophobic Groups Contribute Equally to the Binding of Hyperactive Antifreeze and Ice-Nucleating Proteins to Ice. *J. Am. Chem. Soc.* **2019**, *141*, 7887–7898.

(42) Nutt, D. R.; Smith, J. C. Dual Function of the Hydration Layer around an Antifreeze Protein Revealed by Atomistic Molecular Dynamics Simulations. *J. Am. Chem. Soc.* **2008**, *130*, 13066–13073.

(43) Grabowska, J.; Kuffel, A.; Zielkiewicz, J. Role of the Solvation Water in Remote Interactions of Hyperactive Antifreeze Proteins with the Surface of Ice. *J. Phys. Chem. B* **2019**, *123*, 8010–8018.

(44) Biswas, A. D.; Barone, V.; Daidone, I. High Water Density at Non-Ice-Binding Surfaces

Contributes to the Hyperactivity of Antifreeze Proteins. *J. Phys. Chem. Lett.* **2021**, *12*, 8777–8783.

(45) Lukas, M.; Schwidetzky, R.; Kunert, A. T.; Backus, E. H.; Pöschl, U.; Fröhlich-Nowoisky, J.; Bonn, M.; Meister, K. Interfacial Water Ordering Is Insufficient to Explain Ice-Nucleating Protein Activity. *J. Phys. Chem. Lett.* **2021**, *12*, 218–223, Publisher: American Chemical Society.

(46) Pandey, R.; Usui, K.; Livingstone, R. A.; Fischer, S. A.; Pfaendtner, J.; Backus, E. H. G.; Nagata, Y.; Fröhlich-Nowoisky, J.; Schmüser, L.; Mauri, S.; Scheel, J. F.; Knopf, D. A.; Pöschl, U.; Bonn, M.; Weidner, T. Ice-nucleating bacteria control the order and dynamics of interfacial water. *Science Advances* **2016**, *2*, e1501630.

(47) Roeters, S. J.; Golbek, T. W.; Bregnhøj, M.; Drace, T.; Alamdari, S.; Roeboom, W.; Kramer, G.; Šantl Temkiv, T.; Finster, K.; Pfaendtner, J.; Woutersen, S.; Boesen, T.; Weidner, T. Ice-nucleating proteins are activated by low temperatures to control the structure of interfacial water. *Nat Commun* **2021**, *12*, 1183.

(48) Patel, A. J.; Varilly, P.; Chandler, D. Fluctuations of Water near Extended Hydrophobic and Hydrophilic Surfaces. *J. Phys. Chem. B* **2010**, *114*, 1632–1637.

(49) Rego, N. B.; Xi, E.; Patel, A. J. Identifying hydrophobic protein patches to inform protein interaction interfaces. *Proceedings of the National Academy of Sciences* **2021**, *118*, e2018234118.

(50) Rego, N. B.; Patel, A. J. Understanding Hydrophobic Effects: Insights from Water Density Fluctuations. *Annual Review of Condensed Matter Physics* **2022**, *13*, 303–324.

(51) Sinha, I.; Garde, S.; Cramer, S. M. Comparative Analysis of Protein Surface Hydrophobicity Maps Determined by Sparse Sampling INDUS and Spatial Aggregation Propensity. *J. Phys. Chem. B* **2023**, *127*, 10304–10314.

(52) Patel, A. J.; Garde, S. Efficient Method To Characterize the Context-Dependent Hydrophobicity of Proteins. *J. Phys. Chem. B* **2014**, *118*, 1564–1573.

(53) Godawat, R.; Jamadagni, S. N.; Garde, S. Characterizing hydrophobicity of interfaces by using cavity formation, solute binding, and water correlations. *Proceedings of the National Academy of Sciences* **2009**, *106*, 15119–15124.

(54) Acharya, H.; Vembanur, S.; Jamadagni, S. N.; Garde, S. Mapping hydrophobicity at the nanoscale: Applications to heterogeneous surfaces and proteins. *Faraday Discuss.* **2010**, *146*, 353–365.

(55) Xi, E.; Venkateshwaran, V.; Li, L.; Rego, N.; Patel, A. J.; Garde, S. Hydrophobicity of proteins and nanostructured solutes is governed by topographical and chemical context. *Proceedings of the National Academy of Sciences* **2017**, *114*, 13345–13350.

(56) Marks, S. M.; Vicars, Z.; Thosar, A. U.; Patel, A. J. Characterizing Surface Ice-Philicity Using Molecular Simulations and Enhanced Sampling. *J. Phys. Chem. B* **2023**, *127*, 6125–6135.

(57) Lechner, W.; Dellago, C. Accurate determination of crystal structures based on averaged local bond order parameters. *J. Chem. Phys.* **2008**, *129*, 114707.

(58) Patel, A. J.; Varilly, P.; Chandler, D.; Garde, S. Quantifying Density Fluctuations in Volumes of All Shapes and Sizes Using Indirect Umbrella Sampling. *J Stat Phys* **2011**, *145*, 265–275.

(59) Abascal, J. L. F.; Sanz, E.; García Fernández, R.; Vega, C. A potential model for the study of ices and amorphous water: TIP4P/Ice. *J. Chem. Phys.* **2005**, *122*, 234511.

(60) Miyamoto, S.; Kollman, P. A. Settle: An analytical version of the SHAKE and RATTLE algorithm for rigid water models. *Journal of Computational Chemistry* **1992**, *13*, 952–962.

(61) Essmann, U.; Perera, L.; Berkowitz, M. L.; Darden, T.; Lee, H.; Pedersen, L. G. A smooth particle mesh Ewald method. *J. Chem. Phys.* **1995**, *103*, 8577–8593.

(62) Bussi, G.; Donadio, D.; Parrinello, M. Canonical sampling through velocity rescaling. *J. Chem. Phys.* **2007**, *126*, 014101.

(63) Bernetti, M.; Bussi, G. Pressure control using stochastic cell rescaling. *The Journal of Chemical Physics* **2020**, *153*, 114107.

(64) Parrinello, M.; Rahman, A. Polymorphic transitions in single crystals: A new molecular dynamics method. *Journal of Applied physics* **1981**, *52*, 7182–7190.

(65) Tan, Z.; Gallicchio, E.; Lapelosa, M.; Levy, R. M. Theory of binless multi-state free energy estimation with applications to protein-ligand binding. *J Chem Phys* **2012**, *136*.

(66) Zhu, F.; Hummer, G. Convergence and error estimation in free energy calculations using the weighted histogram analysis method. *J Comput Chem* **2012**, *33*, 453–465.

(67) Shirts, M. R.; Chodera, J. D. Statistically optimal analysis of samples from multiple equilibrium states. *J Chem Phys* **2008**, *129*, 124105.

(68) Matsumoto, M.; Yagasaki, T.; Tanaka, H. GenIce: Hydrogen-Disordered Ice Generator. *Journal of Computational Chemistry* **2018**, *39*, 61–64.

(69) Arblaster, J. W. *Selected Values of the Crystallographic Properties of Elements*; A S M International: Materials Park, UNITED STATES, 2018.

(70) Leinala, E. K.; Davies, P. L.; Doucet, D.; Tyshenko, M. G.; Walker, V. K.; Jia, Z. A β-helical antifreeze protein isoform with increased activity: structural and functional insights. *Journal of biological chemistry* **2002**, *277*, 33349–33352.

(71) Hornak, V.; Abel, R.; Okur, A.; Strockbine, B.; Roitberg, A.; Simmerling, C. Comparison of multiple AMBER force fields and development of improved protein backbone parameters. *Proteins* **2006**, *65*, 712–725.

(72) Rego, N. B.; Xi, E.; Patel, A. J. Protein hydration waters are susceptible to unfavorable perturbations. *Journal of the American Chemical Society* **2019**, *141*, 2080–2086.

(73) Rego, N. B.; Ferguson, A. L.; Patel, A. J. Learning the relationship between nanoscale chemical patterning and hydrophobicity. *Proceedings of the National Academy of Sciences* **2022**, *119*, e2200018119.

(74) Fitzner, M.; Sosso, G. C.; Cox, S. J.; Michaelides, A. The Many Faces of Heterogeneous Ice Nucleation: Interplay Between Surface Morphology and Hydrophobicity. *J. Am. Chem. Soc.* **2015**, *137*, 13658–13669.

(75) Pedevilla, P.; Fitzner, M.; Sosso, G. C.; Michaelides, A. Heterogeneous seeded molecular dynamics as a tool to probe the ice nucleating ability of crystalline surfaces. *J. Chem. Phys.* **2018**, *149*, 072327.

(76) Yuan, T.; DeFever, R. S.; Zhou, J.; Cortes-Morales, E. C.; Sarupria, S. RSeeds: Rigid Seeding Method for Studying Heterogeneous Crystal Nucleation. *J. Phys. Chem. B* **2023**, *127*, 4112–4125.

(77) Graether, S. P.; Kuiper, M. J.; Gagné, S. M.; Walker, V. K.; Jia, Z.; Sykes, B. D.; Davies, P. L. β-Helix structure and ice-binding properties of a hyperactive antifreeze protein from an insect. *Nature* **2000**, *406*, 325–328.

(78) Hudait, A.; Qiu, Y.; Odendahl, N.; Molinero, V. Hydrogen-bonding and hydrophobic groups contribute equally to the binding of hyperactive antifreeze and ice-nucleating proteins to ice. *Journal of the American Chemical Society* **2019**, *141*, 7887–7898.

(79) Kapcha, L. H.; Rossky, P. J. A simple atomic-level hydrophobicity scale reveals protein interfacial structure. *Journal of molecular biology* **2014**, *426*, 484–498.

(80) Graham, L. A.; Liou, Y.-C.; Walker, V. K.; Davies, P. L. Hyperactive antifreeze protein from beetles. *Nature* **1997**, *388*, 727–728.

(81) Davies, P. L. Ice-binding proteins: a remarkable diversity of structures for stopping and starting ice growth. *Trends in biochemical sciences* **2014**, *39*, 548–555.

(82) Liu, K.; Wang, C.; Ma, J.; Shi, G.; Yao, X.; Fang, H.; Song, Y.; Wang, J. Janus effect of antifreeze proteins on ice nucleation. *Proceedings of the National Academy of Sciences* **2016**, *113*, 14739–14744.

(83) Prakash, S.; Xi, E.; Patel, A. J. Spontaneous recovery of superhydrophobicity on nanotextured surfaces. *PNAS* **2016**, *113*, 5508–5513.

(84) Baran, L.; Llombart, P.; Rżysko, W.; MacDowell, L. G. Ice friction at the nanoscale. *Proceedings of the National Academy of Sciences* **2022**, *119*, e2209545119.

(85) Luengo-Márquez, J.; Izquierdo-Ruiz, F.; MacDowell, L. G. Intermolecular forces at ice and water interfaces: Premelting, surface freezing, and regelation. *J. Chem. Phys.* **2022**, *157*, 044704.

(86) Louden, P. B.; Gezelter, J. D. Friction at Ice-Ih/Water Interfaces Is Governed by Solid/Liquid Hydrogen-Bonding. *J. Phys. Chem. C* **2017**, *121*, 26764–26776.

(87) Louden, P. B.; Gezelter, J. D. Why is Ice Slippery? Simulations of Shear Viscosity of the Quasi-Liquid Layer on Ice. *J. Phys. Chem. Lett.* **2018**, *9*, 3686–3691.

(88) Khurana, M.; Yin, Z.; Linga, P. A Review of Clathrate Hydrate Nucleation. *ACS Sustainable Chem. Eng.* **2017**, *5*, 11176–11203.

(89) Thakre, N.; Jana, A. K. Physical and molecular insights to Clathrate hydrate thermodynamics. *Renewable and Sustainable Energy Reviews* **2021**, *135*, 110150.

(90) DeFever, R. S.; Sarupria, S. Surface chemistry effects on heterogeneous clathrate hydrate nucleation: A molecular dynamics study. *The Journal of Chemical Thermodynamics* **2018**, *117*, 205–213.

(91) Huard, D. J. E.; Johnson, A. M.; Fan, Z.; Kenney, L. G.; Xu, M.; Drori, R.; Gumbart, J. C.; Dai, S.; Lieberman, R. L.; Glass, J. B. Molecular basis for inhibition of methane clathrate growth by a deep subsurface bacterial protein. *PNAS Nexus* **2023**, *2*, pgad268.

TOC Graphic